ARTICLE

# Reaction of $CH_2Cl$ with $O_2$[†]

Hai-tao Ma, Cong-yun Shi, Wen-sheng Bian, Hong-mei Su, Fan-ao Kong*

*The State Key Laboratory of Molecular Reaction Dynamics, Institute of Chemistry, Chinese Academy of Sciences, Beijing 100080, China*

(Dated: Received on May 26, 2007; Accepted on July 11, 2007)

The elementary reaction of $CH_2Cl+O_2$ in gas phase was investigated by time-resolved FTIR emission spectroscopy. Vibrationally excited products CO ($v\leq4$), and $CO_2$ ($\nu_3$, $v\leq7$) were observed. The yield ratio of $CO/CO_2(\nu_3)$ was 72.2±7. The reaction pathways were studied theoretically at QCISD//UB3LYP/6-311++G(d,p) level. In the beginning of the reaction, $CH_2Cl$ radical associated with $O_2$ to form $CH_2ClOO$, followed by removal of the Cl atom to yield another intermediate dioxirane $CH_2OO$. Subsequently, a series of isomerization and decomposition of the $CH_2OO$ took place, yielding the final products of CO and $CO_2$. The calculated result was in consistent with the experimental observation.

**Key words:** FTIR emission spectroscopy, Vibrationally excited product, QCISD

## I. INTRODUCTION

Chlorine containing radicals play a significant role in atmospheric chemistry, such as stratospheric ozone depletion, incineration, and high-temperature pyrolysis of chlorocarbon polymers [1-3]. High-temperature pyrolysis is used as the primary means of disposal of large quantities of polymeric waste. Inevitably, a large number of halogenated alkyl radicals are generated through pyrolysis or complex chain reactions. The halogenated alkyl radicals are toxic and relevant to environmental issues such as stratospheric ozone depletion [2,3]. Therefore, the reactions of halogenated radicals have received considerable interest in recent years. Among those, the oxidations of the halogenated methyl radicals by oxygen are very important [4]. Previous reports on the reaction of the chlorinated methyl radicals ($CCl_3$, $CHCl_2$, $CH_2Cl$) with oxygen are concentrated on the kinetic studies [5-13]. The reaction dynamics between the partially substituted species $CH_2Cl$ and $O_2$ was studied. To our knowledge, very few investigations have been carried out on the reaction so far. The rate constant was determined as $(2.9\pm0.2)\times10^{-12}(T/300)^{-1.2\pm0.4}$ $cm^3/(molecule\ s)$ over the high-pressure range of 2.67 kPa to 101 kPa and as $(1.88\pm0.05)\times10^{-30}(T/300)^{-3.2\pm0.2}$ $cm^6/(molecule^2\ s)$ over the low-pressure range of 133 Pa to 1.33 kPa in nitrogen by Fenter and co-workers [13]. Enthalpy value ($\Delta H^\circ_{298}$=121.7±10.4 kJ/mol) for the addition reaction $CH_2Cl+O_2\rightarrow CH_2ClO_2$ is obtained in the third-law treatment by Knyazev and Slagle [14].

Unfortunately, it is lack of the knowledge of products, pathway and mechanism of the titled reaction in the literatures as far. In the present work, the $CH_2Cl+O_2$ reaction was investigated both experimentally and theoretically. The time-resolved Fourier transform infrared (TR-FTIR) emission spectroscopy was used to determine the reaction products and reaction channels. Vibrationally excited reaction products CO, $CO_2$ were found for the first time. Vibrational energy disposals in $CO_2$ and CO were obtained by spectral simulations. Quantum chemistry calculations were also performed to investigate reaction pathways at the QCISD//UB3LYP/6-311++G(d,p) level. The reaction mechanism of $CH_2Cl+O_2$ has been clarified.

## II. EXPERIMENTAL AND THEORETICAL METHODS

The experimental apparatus was described in detail elsewhere [15]. Briefly, the apparatus consists of a KrF Laser (∼150 mJ/pulse, Lambda Physik-305i), a stainless reaction chamber, and a TR-FTIR spectroscope (Nicolet, Nexus 870). $CH_2Cl$ radical was produced via laser photolysis of $CH_2ClBr$ at 248 nm [16]. The laser beam was led into the reaction chamber. A mixed gas of precursor $CH_2ClBr$ and oxygen flowed through the reaction chamber. The partial pressures of $CH_2ClBr$ and $O_2$ were maintained at 20 and 90 Pa, respectively. The infrared emission was collected by a pair of gold-coated spherical mirrors and was detected and recorded by an InSb (77 K) detector, which is sensitive in the region of 1800-6000 $cm^{-1}$. The time resolution of the transient recorder is 10 μs, and the spectral resolution of the spectroscope is set at 16 $cm^{-1}$. The $CH_2ClBr$ (Aldrich, 97%) was used without purification.

The detailed reaction mechanism was theoretically explored by DFT method in Gaussian 03 program package [17]. UB3LYP/6-311++G(d,p) were employed to locate all the stationary points along the reaction pathways. Full optimisation and vibrational analysis were done for the stationary points on the reaction profile.

[†]Part of the special issue "Cun-hao Zhang Festschrift".

*Author to whom correspondence should be addressed. E-mail: kong@iccas.ac.cn, Fax: +86-10-62563167

 

In order to explicitly establish the relevant species, connections of the transition states between designated reactants and products were confirmed by intrinsic reaction coordinate (IRC) calculations at the same level [18]. It was beyond our present computational feasible to perform higher full optimisation calculations for all stationary points, so to yield more accurate energetic information, only higher level single-point energy calculations were performed based on quadratic configuration interaction with single and double excitations (QCISD) using the UB3LYP/6-311++G(d,p) optimized geometries. The zero point energy obtained at UB3LYP/6-311++G(d,p) was included for QCISD /6-311++G(d,p) energy calculations without scaling.

## III. RESULTS AND DISCUSSION

### A. Reaction products

Laser photolysis of pure $CH_2ClBr$ at 248 nm does not result in any emission peak in the TR-FTIR spectrum, so that neat IR emission background is provided for the spectroscopic investigation of the $CH_2Cl+O_2$ reaction (Fig.1(a)). Once the gaseous mixture of $CH_2ClBr$ and $O_2$ is irradiated by the KrF laser, several IR bands appeared in the emission spectrum. Two spectra at 10 and 160 μs after the laser firing were recorded and shown in Fig.1 (b) and (c). The emission between 2170 and 2400 $cm^{-1}$ is assigned as the $v\rightarrow v-1$ transition of $CO_2$

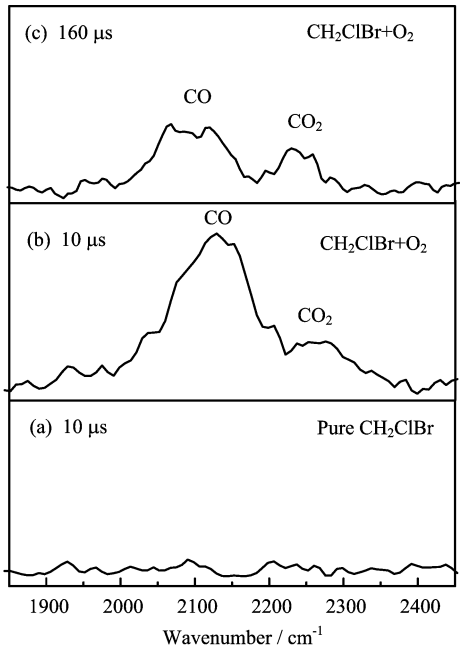


FIG. 1 Time-resolved IR emission spectra for the reaction $CH_2Cl+O_2$. The delay time after the KrF laser firing. The partial pressures of $CH_2ClBr$ and $O_2$ are 20 and 90 Pa, respectively.

$\nu_3$ mode (The $\nu_1$, $\nu_2$ bands of $CO_2$ are not observable in the present IR spectrum). Another emission between 1900 and 2250 $cm^{-1}$ is attributed to the $v\rightarrow v-1$ transition of CO. Due to quenching effect, the two emission bands separate from each other in the spectra at 160 μs.

Tzeng *et al.* reported that the photodissociation of $CH_2ClBr$ at 248 nm produced $CH_2Cl$ exclusively [16]. This point is also confirmed by our measurement of the laser fluence dependence. A linear laser fluence dependence of the CO and $CO_2$ yields was measured in the experimental work. The total yield at 10 μs increases gradually with the increasing of laser intensity as shown in Fig.2. The slope in Fig.2 is 1.0±0.20, which indicates that the products CO and $CO_2$ are yielded from one-photon photolysis. The one-photon photolysis of $CH_2ClBr$ can generate $CH_2Cl$ radical merely, but not $CH_2$ radical which is the two-photon photolytic product. Therefore, the CO and $CO_2$ observed in this experiment are the products of $CH_2Cl+O_2$ reaction.

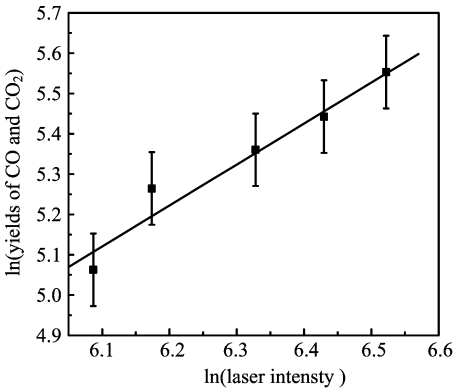


FIG. 2 Laser intensity dependence of the total yields of CO and $CO_2$ with the slope of 1.0±0.20.

### B. Vibrational energy disposal in $CO_2(\nu_3)$ and CO

#### 1. Spectral simulation method

The vibrational energy disposal of the products can be analyzed by fitting the IR spectra using a nonlinear fitting program which has been described in detail elsewhere [19], and only a brief outline of the scheme was given here. The parameters are determined using the nonlinear least-squares method of Levenbery-Marquardt.

The vibrational population was evaluated by the fitting of the simulated spectrum to the experimental one. The spectral intensity of each rotational line was calculated as

$$I_{v,J\rightarrow v'J'} = \frac{2C_e v^4}{Q^r} S_J^{\mathrm{P.Q.R}} \exp\left[-B'J'(J'+1)\frac{hc}{kT_r}\right] \quad (1)$$

where $C_e$ is a constant, $v$, $Q_\mathrm{r}$, $T_\mathrm{r}$, $S_J^{\mathrm{P.Q.R}}$ are the emission frequency, the rotational partition function, the ro-

DOI:10.1088/1674-0068/20/04/383-387 

TABLE I Populations of the products (CO and $CO_2$) of reaction $CH_2Cl+O_2$ at different vibrational levels (10 μs, $CO/CO_2$=72.2±7)

| Population | $v$=1 | $v$=2 | $v$=3 | $v$=4 | $v$=5 | $v$=6 | $v$=7 |
|---|---|---|---|---|---|---|---|
| CO | 252±30 | 140±15 | 132±11 | 51±6 | – | – | – |
| $CO_2(\nu_3)$ | 1.20±0.20 | 1.71±0.20 | 1.14±0.12 | 1.18±0.12 | 1.48±0.15 | 1.17±0.12 | 0.04±0.004 |

tational temperature and the Honl-London factor, respectively. For a specific rovibrational state, $2C_e v^4/Q_r$ is approximately a constant. Therefore, the intensity is dependent mainly upon $S_J^{P,Q,R}\exp[-B'J'(J'+1)hc/kT_r]$.

In addition, an instrumental function $\Delta\mathrm{sinc}^2(\pi v\Delta)$ has been used as instrumental line shape (ILS) to broaden the rovibrational line in the fitting, where $\Delta$ is the largest difference of the optical path length. For a specific vibrational transition $v\rightarrow v-1$, the emission intensity function $f_v(v)$ can be obtained by convoluting the rovibonic lines with the ILS function. The overall simulated spectrum $I_n(v)$ is the sum of the individual vibrational bands weighted by the population $N_v$ over all frequencies.

$$I_n(v) = \Sigma_v N_v A_v v_v f_v \tag{2}$$

$A_v$ is the Einstein spontaneous radiation coefficient for the transition of $v\rightarrow v-1$ transition. $v_v$ is the frequency for $v\rightarrow v-1$ transition.

The $A(v,J)$ values for CO are calculated by the formula [20]

$$A(s^{-1}) = \frac{64\pi^4}{3h}v^3\frac{|m|}{2J'+1}\langle vJ|m|v'J'\rangle^2 \tag{3}$$

Where the $\langle vJ|m|v'J'\rangle$ is the dipole transition matrix elements in Debye; $m$ is equal to $J$+1 for the $R$ lines and to $J$ for the $P$ lines.

For $CO_2$ molecules, the $A(v,J)$ coefficients are calculated by the formula [21]

$$A(s^{-1}) = \frac{64\pi^4}{3h}v^3\frac{|m|}{2J'+1}|R_{v_3'\rightarrow v_3}|^2F(m) \tag{4}$$

The vibrational transition moment $|R_{v_3'\rightarrow v_3}|^2 = v_3'|R_{1\rightarrow 0}|^2$ have a precise approximation of $|R_{v_3'\rightarrow v_3}|^2 = 0.1032$ Debye$^2$. The Herman-Wallis factor is $F(m) = (1-1.43\times10^4 m)^2$.

Minimizing the square of the difference between the data of $I_n(v)$ and the experimental spectral intensity by adjusting the rotational temperature, the phase error, the highest rotational quantum number, the highest vibrational quantum number, and so on, the vibrational population $N_v$ was obtained.

### 2. Vibrational disposal

Vibrational energy disposal of the products was obtained by simulating the IR spectra of reaction products. The spectra of 10-μs delay was simulated (Fig.3).

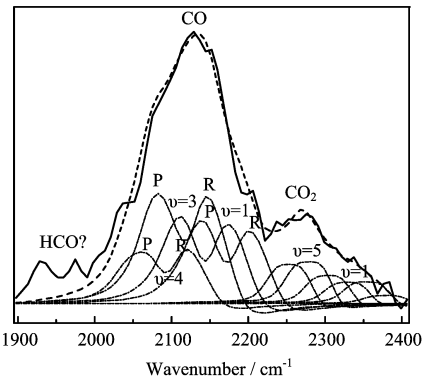


FIG. 3 Simulation of the CO and $CO_2$ spectra in the reaction $CH_2Cl+O_2$ at a 10-μs after laser firing. The experimental spectra are shown by the solid line and the dashed contours are the simulated overall spectra. The dotted curves denote the contributions of the individual $v\rightarrow v-1$ transitions. The best-fit rotational temperatures were found to be 300 K for CO and $CO_2$.

Table I presents the relative vibrational populations of CO and $CO_2$. The best-fitted rotational temperature was 300 K. This result is reasonable if we consider that the rotational excitation of the nascent products has almost been quenched at the pressure of 110 Pa within 10 μs. However, vibrational quenching is not significant during this period. The $CO_2$ products are highly vibrationally excited. The highest vibrational excited level of product $CO_2(\nu_3)$ is $v$=7. And the population is inverse at $v$=2.

The product CO is also vibrationally excited. The highest level populated is $v$=4, which is much lower than that of product $CO_2(\nu_3)$.

Because the populations are normalized by Einstein coefficients [20,21], the yields of the products can be compared. The yield of CO is estimated to be 72 times greater than the yield of $CO_2$ ($\nu_3$) (Shown in Table I). The observation shows that CO is the major product. The vibrational ground state is not included.

### C. Reaction mechanism

To understand the reaction mechanism, we made quantum chemistry calculations. Figure 4 shows the potential energy surface (PES) for the $CH_2Cl+O_2$ reaction pathways. The left part of the energy diagram (solid lines) is calculated in this work at the level of QCISD//UB3LYP/6-311++G(d,p). The right part of the diagram (dotted lines) is adapted from

DOI:10.1088/1674-0068/20/04/383-387 

TABLE II The energies of species (reactant, intermediates, transition states and products) in kJ/mol at UB3LYP/6-311++G(d,p) level

| Species | $\Delta E_0$ | Zero point energy | $H^{\circ}_{298}$ | Relative energy[a] |
|---|---|---|---|---|
| $CH_2Cl+O_2$ | 0.0 (−2718.3318)[b] | 0.0 (0.110117) | 0.0 (−2718.18928) | 0.0 (−2714.0450) |
| IM1 | −119.21 | 21.17 | −104.41 | −119.30 |
| IM2 | −114.87 | 20.16 | −100.56 | −115.45 |
| TS1 | 101.23 | 17.99 | 112.23 | 153.10 |
| IM3+Cl | 23.76 | 15.98 | 35.97 | 11.80 |

[a] At QCISD//UB3LYP/6-311++G (d,p) level, including the zero point energy obtained at UB3LYP/6-311++G (d,p) without scaling.
[b] Values in parenthesis are in hartree.

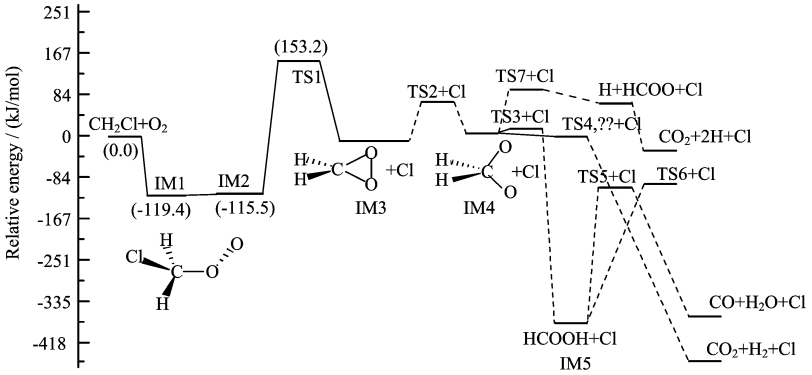


FIG. 4 Energy scheme for the $CH_2Cl+O_2$ reaction. The left portion of the scheme (connected by solid lines) are calculated at the QCISD//UB3LYP/6-311G++(d,p) levels. The right portion of the scheme (connected by dotted lines) are adapted from Ref.[19].

Ref.[22], in which the energies were calculated at the CASSCF/CASPT2 level. The geometries of reactant, intermediate IM1 and its isomer IM2 and transition state TS1 are shown in Fig.5.

At the beginning of the reaction, the $CH_2Cl$ radical associates with $O_2$ to form an intermediate $CH_2ClOO$ (IM1). It is a barrierless process, happened within a few collisions. The calculated electronic energy of the intermediate IM1 is 119.2 kJ/mol lower than that of the reactants at QCISD//UB3LYP/6-311++G (d,p) level (See Table II). The calculated value is close to the enthalpy value (−121.7±10.45 kJ/mol) measured by Knyazev and Slagle [14].

Later, the isomerization from IM1 to IM2 changes the dihedral angel Cl−C−O−O from 85.01° to 180.00°. The energy difference between the two isomers is less than 4.2 kJ/mol. The removal of Cl atom from IM2 leads to IM3 via TS1 and this process is one-step concerted reaction, including Cl-elimination and COO three-membered ring formation, which is the rate-determining process of the reaction. The calculation at UB3LYP/6-311++G (d,p) level gives the corresponding energy barrier of 101.23 kJ/mol for this TS1, however, the calculation at QCISD//UB3LYP/6-311++G (d,p) level gives a higher one of 153.10 kJ/mol. The energetic $CH_2Cl$ fragment, which is a radical and formed in the photolysis of $CH_2ClBr$, carries the available energy to overcome the energy barrier, yielding the key intermediate dioxirane $CH_2OO$, IM3. In the later time, a series of isomerization and decomposition may take place with the IM3, yielding the final products CO and $CO_2$. It is noticed that the branching ratio of $CO/CO_2$ is as high as 72. It is interesting that the latter processes are analogous to the reaction of $CH_2+O_2$, which has been investigated in our previous work [22-25]. The final products in both the reactions are CO and $CO_2$. The CO molecule is the main product in both the cases [22].

## IV. CONCLUSION

The reaction of $CH_2Cl$ with $O_2$ was investigated both experimentally and theoretically. The nascent products $CO_2$, CO were found by time-resolved Fourier transform IR emission spectroscopy. The spectra of nascent products were simulated. The highest excitation levels of CO and $CO_2$ ($\nu_3$) are $v$=4 and $v$=7, respectively. The reaction channel leading to CO is the major channel. The reaction mechanisms were studied at the QCISD//UB3LYP/6-311++G (d,p) level. $O_2$ molecule attacks $CH_2Cl$ radical to form chloromethyl peroxy radical, which is followed by isomerization, Cl-eliminating

DOI:10.1088/1674-0068/20/04/383-387 

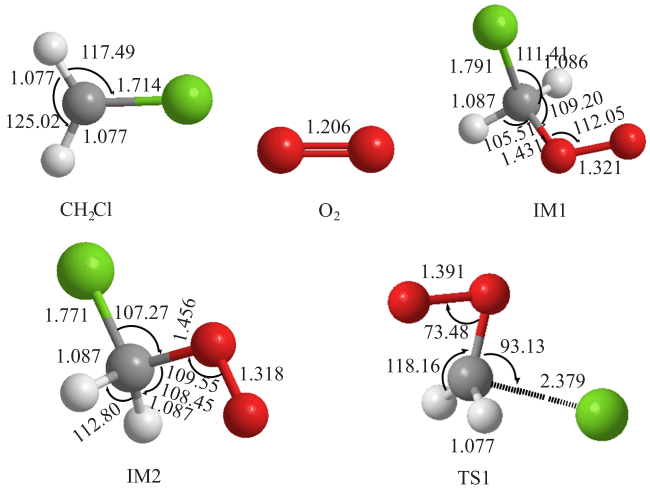


FIG. 5 The optimized geometries of reactants, intermediate and transition state at the level of UB3LYP/6-311++G(d,p). The black, white, green and red balls denote C, H, Cl and O atoms, respectively. The bond lengths are in Å, and the angles are in (°). For interpretation of the color in this figure legend, the reader can refer to the web version of this article.

and COO three-membered ring formation to IM3. Subsequently, final products CO and $CO_2$ are yielded via different reaction pathways. Our experiment and calculation indicate that the major products are CO and $CO_2$. Since the highest barrier is 153.10 kJ/mol higher than the reactants, the reaction dose not occur under the ambient conditions, in consistent with the experimental observation [26-28].

## V. ACKNOWLEDGMENTS

This work was supported by the National Natural Science Foundation of China and the National Key Basic Research Special Funds projects.

[1] H. Hou, B. S. Wang, and Y. S. Gu, J. Phys. Chem. A **103**, 8075 (1999).
[2] World Meteorological Organization, *Global Ozone Research and Monitoring Project*, Report No.20, (1989).
[3] S. M. Senkan, *Detoxification of Hazardous Waste*, Chapter 3, (1982).
[4] T. C. Xiang, K. H. Liu, C. Y. Shi, H. M. Su, and F. A. Kong, Chem. Phys. Lett. **437**, 8 (2007).
[5] R. Cooper, J. B. Cumming, S. Gordon, and W. A. Mulac, Radiat. Phys. Chem. **16**, 169 (1980).
[6] K. R. Ryan and I. C. Plumb. Int. J. Chem. Kinet. **16**, 591 (1984).
[7] J. J. Russell, J. A. Seetula, D. Gutman, F. Danis, F. Caralp, P. D. Lightfoot, R. Lesclaux, C. F. Melius, and S. M. Senkan, J. Phys. Chem. **94**, 3277 (1990).
[8] F. Danis, F. Caralp, M. T. Rayez, and R. Lesclaux, J. Phys. Chem. **95**, 7300 (1991).
[9] F. F. Fenter, P. D. Lightfoot, J. T. Niiranen, and D. Gutmann, J. Phys. Chem. **97**, 5313 (1993).
[10] W. C. Nottingham, R. N. Rudolph, K. P. Andrews, J. H. Moore, and J. A. Tossell, Int. J. Chem. Kinet. **26**, 749 (1994).
[11] K. Luther, K. Oum, and J. Troe, J. Phys. Chem. A **105**, 5535 (2001).
[12] W. Forst and F. Caralp, J. Chem. Soc. Faraday Trans. **87**, 2307 (1991).
[13] F. F. Fenter, P. D. Lightfoot, F. Caralp, R. Lesclaux, J. T. Niiranen, and D. Gutman, J. Phys. Chem. **97**, 4695 (1993).
[14] V. D. Knyazev and I. R. Slagle, J. Phys. Chem. A **102**, 1770 (1998).
[15] Q. H. Zhu, S. L. Huang, X. B. Wang, Z. Hao, Q. F. Zhang, J. R. Cao, X. J. Wu, N. Lv, S. X. Yao, and F. A. Kong, Chin. J. Chem. Phys. **6**, 87 (1993).
[16] W. B. Tzeng, Y. R. Lee, and S. M. Lin, Chem. Phys. Lett. **227**, 467 (1994).
[17] M. J. Frisch, G. W. Trucks, H. B. Schlegel, G. E. Scuseria, M. A. Robb, J. R. Cheeseman, J. A. Montgomery, Jr., T. Vreven, K. N. Kudin, J. C. Burant, J. M. Millam, S. S. Iyengar, J. Tomasi, V. Barone, B. Mennucci, M. Cossi, G. Scalmani, N. Rega, G. A. Petersson, H. Nakatsuji, M. Hada, M. Ehara, K. Toyota, R. Fukuda, J. Hasegawa, M. Ishida, T. Nakajima, Y. Honda, O. Kitao, H. Nakai, M. Klene, X. Li, J. E. Knox, H. P. Hratchian, J. B. Cross, C. Adamo, J. Jaramillo, R. Gomperts, R. E. Stratmann, O. Yazyev, A. J. Austin, R. Cammi, C. Pomelli, J. W. Ochterski, P. Y. Ayala, K. Morokuma, G. A. Voth, P. Salvador, J. J. Dannenberg,V. G. Zakrzewski, S. Dapprich, A. D. Daniels, M. C. Strain, O. Farkas, D. K. Malick, A. D. Rabuck, K. Raghavachari, J. B. Foresman, J. V. Ortiz, Q. Cui, A. G. Baboul, S. Clifford, J. Cioslowski, B. B. Stefanov, G. Liu, A. Liashenko, P. Piskorz, I. Komaromi, R. L. Martin, D. J. Fox, T. Keith, M. A. Al-Laham, C. Y. Peng, A. Nanayakkara, M. Challacombe, P. M. W. Gill, B. Johnson, W. Chen, M. W. Wong, C. Gonzalez, and J. A. Pople, *Gaussian 03, Revision B.01*, Pittsburgh PA: Gaussian, Inc., (2003).
[18] C. Gonzalez and H. B. Schlegel, J. Phys. Chem. **94**, 5523 (1990).
[19] H. M. Su, J. X. Yang, Y. H. Ding, W. H. Feng, and F. A. Kong, Chem. Phys. Lett. **326**, 73 (2000).
[20] C. Jr. Chackerian and R. H. Tipping, J. Mol. Spec. **99**, 431 (1983).
[21] J. W. C. Johns, J. Mol. Spec. **134**, 433 (1989).
[22] B. Z. Chen, J. M. Anglada, M. B. Huang, and F. A. Kong, J. Phys. Chem. A **106**, 1877 (2002).
[23] H. M. Su, W. T. Mao, and F. A. Kong, Chem. Phys. Lett. **322**, 21 (2000).
[24] H. M. Su, W. T. Mao, Y. He, L. X. Xu, Y. Sun, and F. A. Kong, Acta Phys. Chim. Sin. **14**, 597 (1998).
[25] B. Z. Chen, M. B. Huang, H. M. Su, and F. A. Kong, Acta Phys. Chim. Sin. **16**, 869 (2000).
[26] E. Sanhueza and J. L. Heicklen, J. Phys. Chem. **79**, 7 (1975).
[27] M. Bilde, J. Sehested, O. J. Nielsen, and T. J. Wallington, J. Phys. Chem. A **101**, 5477 (1997).
[28] H. Niki, P. D. Maker, C. M. Savage, and L. P. Breitenbach, Int. J. Chem. Kinet. **12**, 1001 (1980).

DOI:10.1088/1674-0068/20/04/383-387 